

# Bifurcation diagram of a complex delay-differential equation with cubic nonlinearity

D. Pieroux and Paul Mandel

*Optique Nonlinéaire Théorique, Université Libre de Bruxelles, Campus Plaine, Code Postale 231, 1050 Bruxelles, Belgium*

(Received 13 August 2002; published 21 May 2003)

We reduce the Lang-Kobayashi equations for a semiconductor laser with external optical feedback to a single complex delay-differential equation in the long delay-time limit. The reduced equation has a time-delayed linear term and a cubic instantaneous nonlinearity. There are only two parameters, the real linewidth enhancement factor and the complex feedback strength. The equation displays a very rich dynamics and can sustain steady, periodic, quasiperiodic, and chaotic regimes. We study the steady solutions analytically and analyze the periodic solutions by using a numerical continuation method. This leads to a bifurcation diagram of the steady and periodic solutions, stable and unstable. We illustrate the chaotic regimes by a direct numerical integration and show that low frequency fluctuations still occur.

DOI: 10.1103/PhysRevE.67.056213

PACS number(s): 05.45.-a, 02.30.Ks, 42.65.Sf

## I. INTRODUCTION

Since the work of Verhulst (1804–1849) in population dynamics, delay-differential equations (DDEs) are used to model dynamical systems in many scientific and engineering domains, e.g., optics [1,2], chemistry [3,4], climatology [5,6], biology [7,8], car traffic [9,10], economy [11,12], and cryptosystems based on synchronized hyperchaos [13–16]. Their widespread use stems from the fact that delayed terms handle two common situations. First, they mimic in a simplistic way the time required for a component of the model to switch between two states. Second, a time lag results naturally from the finite propagation velocity of substances [17] and energy fields [1,2,18], as well as from the latency of feedback loops [19].

In this paper, we focus our attention on the dynamics generated by the simple DDE

$$\frac{dE}{dt} = -(1 + i\alpha)|E|^2 E + \chi E(t-1). \quad (1)$$

All variables and parameters in Eq. (1) are dimensionless.  $E(t)$  is a complex variable,  $t$  is the time, and  $\alpha$  and  $\chi$  are real parameters. This equation has an instantaneous cubic nonlinearity  $|E|^2 E$  and a linear delayed term  $E(t-1)$ . These two terms are necessary for the system to display an interesting dynamics: if  $\chi=0$ ,  $E(t)$  vanishes in the long time limit, while removing the nonlinearity leads to a linear equation whose long term solution either vanishes or diverges. The coefficient  $\alpha$  couples the phase and amplitude of  $E$ . Most of the results will be derived for real  $\chi$ . However, some bifurcation mechanisms are easier to understand, and some proofs are made simpler if  $\chi$  is complex. This is achieved by writing  $\chi = \eta e^{-i\Omega}$  with  $\eta$  and  $\Omega$  real:

$$\frac{dE}{dt} = -(1 + i\alpha)|E|^2 E + \eta e^{-i\Omega} E(t-1). \quad (2)$$

As shown in Sec. II, Eq. (2) models the problem of a semiconductor laser pumped at threshold and subject to an optical feedback with a large delay. However, the interest of

Eq. (2) extends well beyond that particular model. For instance, the complex equation describing the small amplitude oscillations of a system subject to a delayed effect shares a common structure with Eq. (2), as discussed in Refs. [20,21] for the case of real-valued models of class-*B* lasers subject to incoherent optical or optoelectronic feedbacks. Equation (2) has also been investigated in connection with the analysis of experiments conducted on a single-mode CO<sub>2</sub> laser with delayed feedback of the losses [22,23] where a two-dimensional (2D) representation of the time series was proposed. Its justification was given in Ref. [24] where it was proved that close to a Hopf bifurcation of Eq. (2), the solvability condition (i.e., the slowly varying amplitude equation) is a complex Ginzburg-Landau equation with real diffusion. The same result was also obtained for a 2D rate equation model of a laser with external delayed feedback [25]. Similar experiments conducted on a class-*A* He-Ne laser have also relied on an equation similar to Eq. (2) for interpretation [26,27].

In this paper, we focus on the bifurcation diagram for the steady and periodic solutions of Eq. (1). There are two surprising features with this bifurcation diagram: (i) its unexpected complexity and (ii) its similarity with the bifurcation diagram derived for the full Lang-Kobayashi equations [20,28]. The complexity of the bifurcation diagram stems from the bridges that connect the infinite set of periodic solutions. This infinity is a simple and direct consequence of the delay. The bridges appear via the mechanism already described in Ref. [28]. In addition, we describe a new mechanism that generates the bridge destruction. Finally, we follow numerically two branches of chaotic solutions and show that low frequency fluctuations are still supported by Eq. (1). This paper is organized as follows. In Sec. II, we show how to derive Eq. (1) from the Lang-Kobayashi rate equations. In Sec. III, we study analytically the steady solutions and their stability. Section IV is devoted to the periodic solutions whose bifurcation diagram is obtained numerically by using a continuation method. In Sec. V, we report on the occurrence of low frequency fluctuations in the simplified model (1) and, for completeness, on the existence of chaotic attractors.

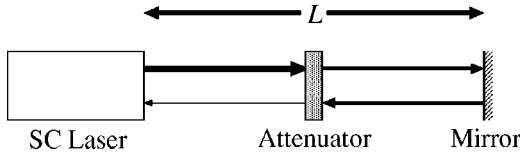


FIG. 1. Schematic setup of a semiconductor laser diode subject to delayed optical feedback. The output beam is reinjected inside the laser cavity after reflection on a mirror. An attenuator is used to reduce the feedback beam intensity. The delay  $\tau$  corresponds to the round-trip time in the external cavity; i.e.,  $\tau=2L/c$ , with  $c$  being the light velocity.

## II. LONG DELAY LIMIT

Lang and Kobayashi [2] proposed a simple rate equation model to describe a semiconductor laser subject to optical feedback (Fig. 1). This model consists of two coupled differential equations for the laser intracavity complex field  $\mathcal{E}$  and the real excess carrier density  $\mathcal{D}$ :

$$\frac{d\mathcal{E}}{dt} = (1 + i\alpha)\mathcal{D}\mathcal{E} + \kappa e^{-i\nu\tau}\mathcal{E}(t-\tau), \quad (3)$$

$$T\frac{d\mathcal{D}}{dt} = P - \mathcal{D} - (1 + 2\mathcal{D})|\mathcal{E}|^2. \quad (4)$$

In these dimensionless equations,  $\alpha$  is the linewidth enhancement factor,  $P$  the excess pump rate above the solitary laser threshold ( $P=0$  at threshold if  $\kappa=0$ ),  $T$  the ratio of the electronic carrier lifetime over the photon lifetime inside the cavity,  $\tau$  the round-trip time outside the laser cavity,  $\kappa \geq 0$  the feedback strength, and  $\nu$  the free-running laser optical frequency. The dimensionless time  $t$  and the delay  $\tau$  are measured in units of the photon lifetime.

Given the complexity of the Lang-Kobayashi equations, it is useful to consider limits in which simplifications may be expected. The obvious parameter on which a limit can be based is the distance between the laser and the external mirror, which controls the delay-time. The short delay time limit has been investigated experimentally and numerically [29–31]. In this paper, we consider the opposite limit of a long delay time. Many experiments on semiconductor lasers focus on pump values close to the solitary laser threshold ( $|P| \ll 1$ ), weak feedback ( $\kappa \ll 1$ ), and large delay ( $\tau \gg 1$ ). To study that range of parameters, we introduce the scaling

$$E = \sqrt{\tau}\mathcal{E}, \quad D = \tau\mathcal{D}, \quad p = \tau P, \quad \eta = \tau\kappa, \quad \Omega = \tau\nu, \quad s = t/\tau. \quad (5)$$

In terms of the scaled variables and parameters, Eqs. (3) and (4) become

$$\frac{dE}{ds} = (1 + i\alpha)DE + \eta e^{-i\Omega}E(s-1), \quad (6)$$

$$\frac{T}{\tau} \frac{dD}{ds} = p - D - \left(1 + \frac{2}{\tau}D\right)|E|^2. \quad (7)$$

In the large delay limit  $\tau \rightarrow \infty$ ,  $(T/\tau)dD/ds$  and  $2D/\tau$  vanish in Eq. (7). The carrier density can then be adiabatically eliminated because Eq. (7) reduces to  $D(t) = p - |E(t)|^2$ . Inserting that result into Eq. (6) and renaming  $s$  by  $t$  leads to a single cubic complex equation for the electric field [32]:

$$\frac{dE}{dt} = (1 + i\alpha)(p - |E|^2)E + \eta e^{-i\Omega}E(t-1). \quad (8)$$

At the solitary laser threshold, i.e., for  $p=0$ , Eq. (2) is recovered.

Before studying the dynamics of Eq. (2), it should be stressed that Eq. (8) is the regular limit of Eqs. (3) and (4) for  $\tau \gg T$  and  $P = O(\tau^{-1})$ . That is, no dynamical phenomenon existing in this parameter domain is lost by simplifying Eqs. (3) and (4) into Eq. (8) and, conversely, every feature of Eq. (8) is also a feature of Eqs. (3) and (4). This may seem contradictory with the fact that Eqs. (3) and (4) can display relaxation oscillations while Eq. (8) cannot. Indeed, in the absence of feedback, the long time solution of Eqs. (3) and (4) is given by

$$\mathcal{E} = \sqrt{P}e^{i\phi}, \quad \mathcal{D} = 0, \quad (9)$$

where  $\phi$  is a constant phase depending on the initial condition. If this stable state is perturbed, the system relaxes with damped relaxation oscillations only if  $8PT > 1$ . Otherwise, the perturbation decays exponentially without oscillations. Because we consider the limit  $\tau \gg T$  and  $P = O(\tau^{-1})$ ,  $8PT \ll 1$  and Eqs. (3) and (4) do not display relaxation oscillations. Thus, the absence of relaxation oscillations in Eq. (8) results from the scaling (5) and the limit  $\tau \gg 1$ ; the full model [Eqs. (6) and (7)] and the reduced model [Eqs. (8) or (2)] share this property.

## III. STEADY SOLUTIONS

In this section, we study analytically the properties of the trivial solution  $E=0$  and of the solutions of Eq. (2) with constant modulus  $|E|$ . Whatever the parameter values,  $E=0$  is always a solution of Eq. (2). A linear stability analysis shows that Hopf bifurcations exist for

$$\Omega_0 = \left(\frac{1}{2} + k\right)\pi + (-1)^k\eta_0, \quad (10)$$

with  $k=0$  or  $1$ . We call these bifurcations primary Hopf bifurcations. As seen in Fig. 2, these Hopf bifurcations form lines dividing the polar plane of the complex parameter  $\eta e^{-i\Omega}$  into an infinite number of regions. Each time a Hopf line is crossed, the trivial solution displays a new bifurcation. Together with an analysis of the stability of the trivial solution for  $\eta \ll 1$ , this implies that the trivial solution is stable only inside the innermost region, the black-filled domain close to the origin in Fig. 2.

Using a two-time scale approach, the branch emerging from a primary Hopf bifurcation can be analyzed in the usual way. For that purpose, we define the vicinity of the bifurcation:  $\eta = \eta_0(\Omega_0, k) + \epsilon^2\eta_2$  with  $\epsilon \ll 1$  and  $\eta_2 = \pm 1$ . We also introduce a slow time variable  $\sigma = \epsilon^2 t$  and use the derivative

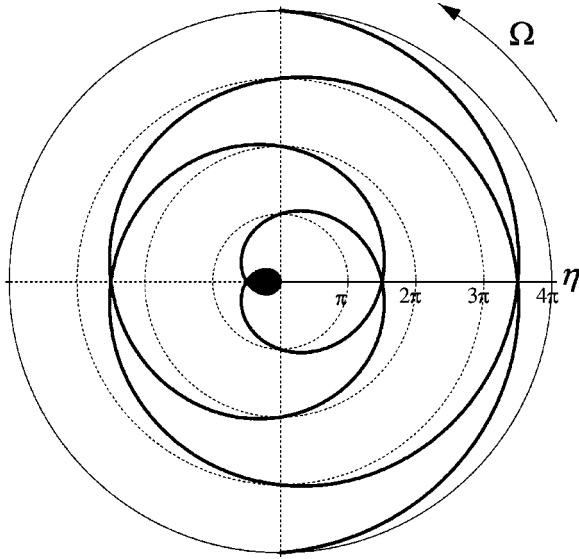


FIG. 2. Location of the primary Hopf bifurcations, Eq. (10). The null solution is stable only in the black-filled innermost domain. Note that for  $\Omega = n\pi$  with  $n$  integer, every  $k=0$  bifurcation collides with a  $k=1$  bifurcation, leading to degenerate Hopf bifurcations. The value of  $\alpha$  is irrelevant here.

chain rule  $d/dt = \partial_t + \epsilon^2 \partial_\sigma$ . Introducing these expressions into Eq. (2) and looking for a perturbed solution of the form

$$E(t) = \epsilon E_1(t, \sigma) + \epsilon^2 E_2(t, \sigma) + \dots, \quad (11)$$

we obtain a cascade of nested problems, one for each power of  $\epsilon$ . Solving the first-order problem gives

$$E_1(t, \sigma) = \rho_1(\sigma) e^{i[\phi_1(\sigma) + \omega_1 t]}, \quad (12)$$

with  $\omega_1 = (-1)^{k+1} \eta_0$ . The slowly varying variables  $\rho_1(\sigma)$  and  $\phi_1(\sigma)$  are determined by a solvability condition obtained at order  $\epsilon^3$ :

$$\frac{d\rho_1}{d\sigma} = \rho_1 \frac{\eta_2 \eta_0 - \rho_1^2 [1 - (-1)^k \alpha \eta_0]}{1 + \eta_0^2}, \quad (13)$$

$$\frac{d\phi_1}{d\sigma} = (-1)^{k+1} \frac{\eta_2 + \rho_1^2 [\eta_0 + (-1)^k \alpha]}{1 + \eta_0^2}. \quad (14)$$

The steady solution is given by

$$\rho_{1,\text{st}}^2 = \frac{\eta_2 \eta_0}{1 - (-1)^k \alpha \eta_0}, \quad (15)$$

$$\phi_{1,\text{st}} = \frac{\eta_2 \sigma}{\alpha \eta_0 - (-1)^k}. \quad (16)$$

For  $k=0$  and  $\alpha \eta_0 > 1$ ,  $\rho_{1,\text{st}}^2 \geq 0$  implies  $\eta_2 = -1$ , and the branch of solutions emerging from the Hopf bifurcation is subcritical. For  $k=1$  or  $\alpha \eta_0 < 1$ ,  $\eta_2 = 1$ , and the branch is supercritical. By linearizing Eq. (13) around the steady solution (15), it is straightforward to show that solutions (15) and

(16) are stable only for supercritical branches emerging at the border of the innermost region of Fig. 2 where the trivial solution is stable. Note that the primary Hopf bifurcations are not degenerated unless  $\Omega$  is a multiple of  $\pi$ . In that case, a  $k=0$  and a  $k=1$  bifurcation coalesce to produce a degenerate bifurcation of the trivial solution.

The solutions emerging from the primary Hopf bifurcations are of the form  $E = \rho_s \exp(i\omega_s t)$ . These solutions are called external cavity modes in the Lang-Kobayashi problem. They are also often referred to as the steady state solutions of Eq. (2) because the corresponding intensity  $|E|^2$  is constant in time. Nevertheless, it should be kept in mind that the complex variable  $E$  still has a harmonic time dependence. Inserting  $E = \rho_s \exp(i\omega_s t)$  into Eq. (2) leads to

$$\rho_s^2 = \eta \cos(\omega_s + \Omega), \quad (17)$$

$$\omega_s = -\eta \sqrt{1 + \alpha^2} \sin(\omega_s + \Omega + \arctan \alpha). \quad (18)$$

Without further approximation, Eq. (18) cannot be solved analytically [33]. Each value of  $\omega_s$  verifying Eq. (18), such that  $\cos(\omega_s + \Omega) > 0$ , defines a distinct steady solution. To study its stability, we seek solutions of the form  $E = (\rho_s + \epsilon \tilde{\rho}) \exp[i\omega_s t + i\epsilon \phi(t)]$ , with  $\epsilon$  small and real. After linearizing Eq. (2) around the steady state solution, the solutions are of the form  $\tilde{\rho}(t)$  and  $\phi(t) \propto \exp(\lambda t)$ . This gives a solvability (or characteristic) equation for  $\lambda$ ,

$$0 = \rho_s^4 (1 + \alpha^2) (3e^\lambda + e^{-\lambda} - 4) + 2\rho_s^2 \alpha \omega_s (2e^\lambda + e^{-\lambda} - 3) + \omega_s^2 (e^\lambda + e^{-\lambda} - 2) + 2\rho_s^2 \lambda (2e^\lambda - 1) + \lambda^2 e^\lambda. \quad (19)$$

This transcendental equation admits an infinity of complex roots. Roots with a zero real part indicate a change of stability, except for one root that always vanishes. It reflects the invariance of the solution with respect to a time translation. For another zero root to exist, the derivative of Eq. (19) with respect to  $\lambda$  must also admit  $\lambda=0$  as a root. This occurs if either  $\rho_s = 0$  or  $1 + \eta \cos(\omega_s + \Omega) = \alpha \eta \sin(\omega_s + \Omega)$ . The first possibility corresponds to the emergence of a steady branch from the trivial solution. The second possibility, together with Eq. (18), corresponds to a turning point. Besides  $\lambda = 0$ , the only other possibility to have a change of stability is a pair of imaginary conjugated roots. Such a pair of roots indicates the existence of a Hopf bifurcation leading to a periodic regime. We call these bifurcations as secondary Hopf bifurcations. Let  $\omega_H$  be the frequency of the periodic oscillation at the secondary Hopf bifurcations. We insert  $\lambda = i\omega_H$  into Eq. (19). Separating real and imaginary parts leads to

$$\omega_H^2 \cos \omega_H + 4\rho_s^2 \omega_H \sin \omega_H = 2[2\rho_s^4 (1 + \alpha^2) + 3\rho_s^2 \alpha \omega_s + \omega_s^2] \times (\cos \omega_H - 1), \quad (20)$$

$$\omega_H^2 \sin \omega_H = 2\rho_s^2 \{ \omega_H (2 \cos \omega_H - 1) + [\rho_s^2 (1 + \alpha^2) + \alpha \omega_s] \sin \omega_H \}. \quad (21)$$

These two equations, coupled to Eqs. (17) and (18), form a system of four equations for the three variables  $\rho_s$ ,  $\omega_s$ , and  $\omega_H$ . Since the system is overdetermined, it is solvable only for particular values of  $\eta = \eta_H(\alpha, \Omega)$  which locate the secondary Hopf bifurcations. Further insight in the existence condition for a secondary Hopf bifurcation is obtained as follows. Let  $\omega_H$  be the oscillation frequency and  $\rho_H$  the amplitude of the steady solution at the secondary Hopf bifurca-

tion. It is then straightforward to express  $\alpha$ ,  $\omega_s$ ,  $\eta$ , and  $\Omega$  in terms of  $\omega_H$ , and  $\rho_H$  as

$$\alpha^2 = \frac{[2\rho_H^4 \sin \omega_H + 2\omega_H \rho_H^2 (2 \cos \omega_H - 1) - \omega_H^2 \sin \omega_H]^2}{2\rho_H^4 [2\rho_H^4 \sin^2 \omega_H + 6\omega_H \rho_H^2 \sin \omega_H + \omega_H^2 (1 + \cos \omega_H)]}, \quad (22)$$

$$\omega_s = -\frac{2\rho_H^4 (1 + \alpha^2) \sin \omega_H + 2\omega_H \rho_H^2 (2 \cos \omega_H - 1) - \omega_H^2 \sin \omega_H}{2\alpha \rho_H^2 \sin \omega_H}, \quad (23)$$

$$\eta^2 = \rho_H^4 (1 + \alpha^2) + 2\alpha \omega_s \rho_H^2 + \omega_s^2, \quad (24)$$

$$\cos^2(\Omega + \omega_s) = \frac{\rho_H^4}{\rho_H^4 (1 + \alpha^2) + 2\alpha \omega_s \rho_H^2 + \omega_s^2}. \quad (25)$$

Because  $\alpha^2 \geq 0$ , Eq. (22) provides an implicit condition that  $\omega_H$  and  $\rho_H$  must also verify

$$2\rho_H^4 \sin^2 \omega_H + 6\omega_H \rho_H^2 \sin \omega_H + \omega_H^2 (1 + \cos \omega_H) < 0. \quad (26)$$

That implies, in particular, the requirement  $\omega_H \sin \omega_H < 0$ . The solution  $E = \rho \exp(i\omega t)$  emerging from a secondary Hopf bifurcations is periodic, i.e.,  $\rho$  and  $\omega$  are periodic in time. In the following section we study these periodic solutions by means of a numerical continuation method because the expressions obtained analytically for  $\rho$  and  $\omega$  are too complicated to be useful.

In this paper, we are following the standard approach to study the secondary Hopf bifurcations. An alternative way to analyze the vicinity of the secondary Hopf bifurcations has been proposed in Ref. [24] where it is shown that a multiple-scale analysis leads to a complex Ginzburg-Landau equation with real diffusion. The occurrence of a partial differential equation in the local analysis of the DDE underpins the complexity of its solutions.

We illustrate the analytical results obtained so far with the bifurcation diagram displayed in Fig. 3(a), shown for  $\alpha = 3$  and  $\Omega = 0$ . The steady branches of constant  $\rho_s = |E|$  are seen to emerge from the trivial solution. Only the supercritical branch emerging from the primary Hopf bifurcation located at the origin  $\eta = 0$  emerges as a stable solution. For  $\Omega \in ]\pi/2, 3\pi/2[ \pmod{2\pi}$ , that solution is shifted from the origin. At all other primary Hopf bifurcations, a pair of subcritical-supercritical branches emerge. This is because a  $k = 0$  primary Hopf bifurcation collides a  $k = 1$  primary Hopf bifurcation for  $\Omega = n\pi$ ,  $n$  being a non-negative integer. The subcritical branches display a turning point after which they become stable. Because all steady branches display an infinite number of secondary Hopf bifurcations, increasing  $\eta$  makes the destabilization of the stable steady solutions ineluctable.

#### IV. PERIODIC SOLUTIONS

Using the numerical continuation package DDEBIFTOOL [34,35] for delay differential dynamical systems, the location and stability of the branches of periodic solutions can be determined. Our results, reported in Fig. 3(a), indicate that the periodic solutions form bridges, at least for moderate values of  $\rho$ . The bridges emerge from the secondary Hopf bifurcations discussed in the preceding section. They always connect a supercritical branch to a subcritical branch. The bridge structure has been recently studied for the Lang-Kobayashi equations (3) and (4) in Refs. [20,28]. In Ref. [20], it was shown that as  $\Omega$  approaches  $n\pi$  from below, every  $k = 0$  primary Hopf bifurcation moves towards a  $k = 1$  primary Hopf bifurcation. At  $\Omega = n\pi$ , they collide and two new secondary bifurcations appear. Increasing  $\Omega$  further, the two primary bifurcations move away from each other while the secondary Hopf bifurcations move up along their steady branches but remain connected by a bridge of periodic solutions (see Fig. 5 in Ref. [20]). As a consequence, secondary bifurcations linked together by a periodic bridge result from the same collision.

From Fig. 3(a) two properties of bridges emerging from a stable steady branch can be found: (i) the periodic branch emerges stably if it is supercritical, and (ii) in the subcritical case, it emerges unstably but becomes stable after a turning point. The other side of the bridge always ends on an unstable steady branch and is unstable. Therefore, there must be a bifurcation on the bridge. It is a tertiary Hopf bifurcation leading to a quasiperiodic regime. This tertiary bifurcation is found on every bridge of periodic solutions, even those who are completely unstable, connecting a supercritical solution and a subcritical solution emerging from the same primary bifurcation. Because the continuation package we use cannot follow quasiperiodic solutions, we integrated Eq. (2) by using a variable step size Runge-Kutta 4(3) method with Hermite interpolation to cope with the delayed term [36]. In this way, we were able to follow the quasiperiodic solutions until they become unstable and lead to a chaotic regime, as shown in Fig. 3(b). Finally, period-doubling bifurcations involving only unstable periodic regimes have been found with the numerical continuation package.

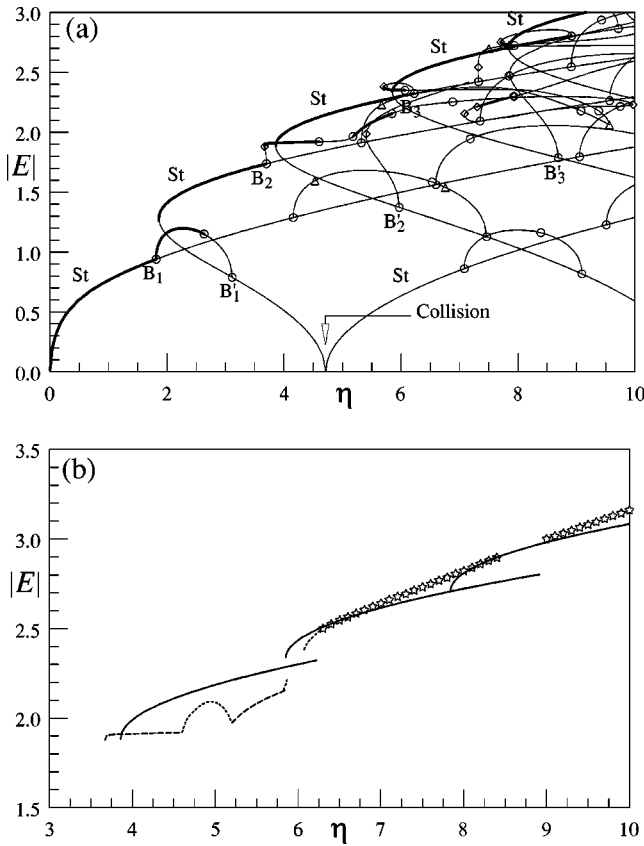


FIG. 3. Bifurcation diagram of Eq. (2) for  $\alpha=3$  and  $\Omega=0$ . The maximum temporal amplitude of  $|E|$  is shown versus the feedback strength  $\eta$ . (a) Diagram obtained via numerical continuation. Thick (thin) lines indicate stable (unstable) solutions. Steady branches are labeled “St,” branches without label are periodic. At  $\eta=3\pi/2$ , there is a collision between a supercritical primary bifurcation and a subcritical primary bifurcation. Circles locate both secondary and tertiary Hopf bifurcations, triangles locate period-doubling bifurcations. Decreasing  $\Omega$  by  $2\pi$  maps the bifurcation points  $B_3, B'_3, B_2,$  and  $B'_2$  onto  $B_2, B'_2, B_1,$  and  $B'_1$ , respectively. (b) Diagram obtained by direct numerical integration of Eq. (2). Steady, periodic, quasiperiodic, and chaotic (including LFF) regimes are drawn with plain lines, dashed lines, dotted lines, and stars, respectively. Unstable solutions are not displayed.

Up to now, we have focused on supercritical-subcritical (sup-sub) collisions, that is, collisions implying a supercritical and a subcritical branch. However, it follows from Eqs. (10) and (15) that if either  $\alpha \leq 2/(3\pi) \approx 0.21$  and  $\Omega = 2n\pi$ , or  $\alpha \leq 2/\pi \approx 0.64$  and  $\Omega = (2n+1)\pi$ , collisions involving two supercritical branches are possible. In Figs. 4(a,b), we show that for  $\alpha=0.5$  and  $\Omega=\pi$  the mechanism leading to the bridge formation is also applicable to the collision of two supercritical branches.

A bridge destruction mechanism has also been identified. Comparing Fig. 4(a) (right before the collision) with Figs. 4(b,c) (right after the collision), it is seen that two secondary Hopf bifurcations  $B_2$  and  $B_3$  have been created on the steady branches, and that they are connected by a bridge of periodic solutions. Increasing  $\Omega$ , the primary bifurcations move apart and the secondary bifurcations move up along the steady

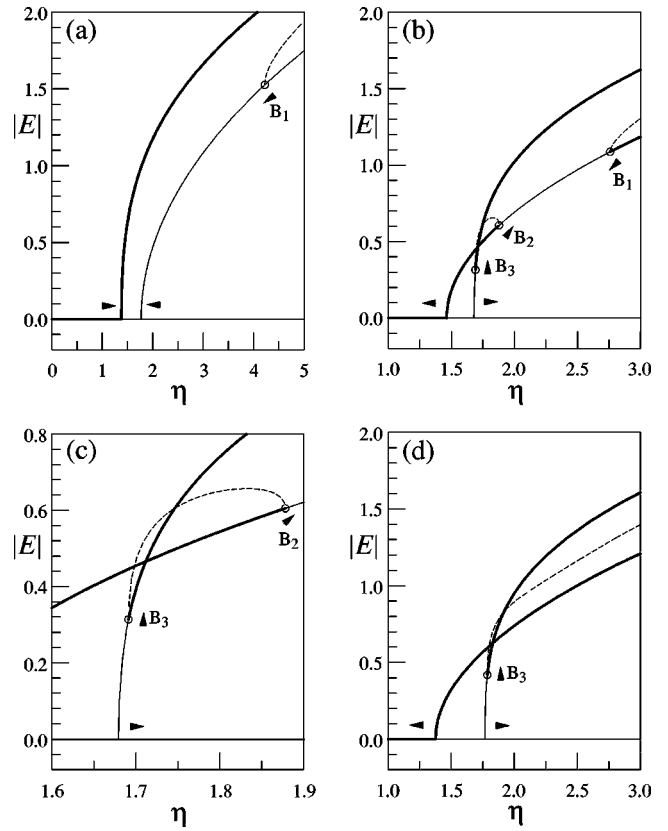


FIG. 4. Details of the bifurcation diagrams of Eq. (2) for  $\alpha=0.5$ , illustrating a collision between two primary supercritical bifurcations while  $\Omega$  is increased. Steady (periodic) regimes are indicated by plain (dashed) lines. Thick (thin) lines indicate stable (unstable) solutions. Circles indicate secondary Hopf bifurcations. The arrows indicate how the branches and the bifurcations move as  $\Omega$  increases. (a)  $\Omega=15\pi/16$ , before the collision. (b),(c)  $\Omega=3.25$ , right after the collision: the two Hopf bifurcations  $B_2$  and  $B_3$  have been created at the collision ( $\Omega=\pi$ ). They sustain a bridge of periodic solutions and move upwards on their respective branches. (d)  $\Omega=17\pi/16$ , bifurcations  $B_1$  and  $B_2$  have collided and disappeared. The bridge is replaced by a periodic solution emerging from  $B_3$ .

branches. This is precisely the scenario for sup-sub collision [20]. However, the bifurcation  $B_2$  collides eventually with a third bifurcation  $B_1$  moving downward on the same steady branch. This collision leads to the disappearance of both  $B_1$  and  $B_2$  bifurcations. At the point of collision, the periodic bridge merges with the branch of periodic solutions associated previously with  $B_1$  [Fig. 4(d)].

Coming back to the question of degeneracy, this analysis shows that for  $\Omega = n\pi + \epsilon$  and  $\epsilon \rightarrow 0$ , two Hopf bifurcations collide if  $\epsilon < 0$ , but four Hopf bifurcations collide if  $\epsilon > 0$ . Thus  $\Omega = n\pi$  is a point of bifurcation collision and discontinuity.

Obvious differences between the sup-sub and sup-sup collisions appear also in the stability of the steady and periodic branches. In the sup-sup case, both ends of the bridges are subcritical, the whole bridge is unstable, and there is no tertiary Hopf bifurcation. Before the primary Hopf bifurcations collide, one steady branch is stable and the other unstable close to zero. After the collision, there has been an exchange

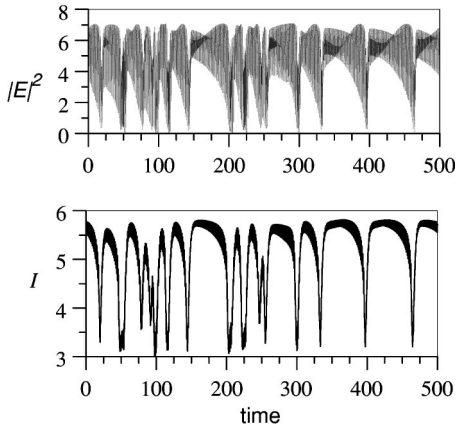


FIG. 5. Unfiltered (upper figure) and low-pass filtered (lower figure) laser intensity using Eq. (1) with  $\eta=7.1$ ,  $\alpha=3$ , and Eq. (27) with  $\tau_F=2$ . The time trace is typical of the chaotic LFF.

of stability and the steady branch emerging from the bifurcation with the smaller value of  $\eta$  is stable except between the bifurcations  $B_1$  and  $B_2$ ; the other steady branch emerges unstable and becomes stable after the bifurcation  $B_3$ .

In the bifurcation diagram displayed in Fig. 3(a), it is seen that the periodic branches have a very complex structure for  $\rho \geq 1.5$ . Nevertheless, the explanation of the bridge formation is still relevant in that domain. Changing  $\Omega$  continuously, all steady and periodic branches move in the diagram, as shown for a limited portion of the diagram in Fig. 4. But after a variation of  $2\pi$ , the bifurcation diagram is back to its original shape since it is shape invariant under the transformation  $\Omega \rightarrow \Omega \pm 2n\pi$ . The secondary Hopf bifurcations move downwards (upwards) on their steady branch as  $\Omega$  decreases (increases). Thus, a periodic branch with a complex structure is mapped onto another periodic branch with smaller  $\rho$  as  $\Omega$  is decreased. For instance, beginning with Fig. 3(a) for  $\Omega=2n\pi$  and reducing  $\Omega$  to  $2(n-1)\pi$ , the secondary Hopf bifurcations labeled  $B_3$  and  $B'_3$  are mapped onto the bifurcation points  $B_2$  and  $B'_2$ , respectively, while the secondary Hopf bifurcations labeled  $B_2$  and  $B'_2$  are mapped onto the bifurcation points  $B_1$  and  $B'_1$ , respectively. This suggests that the branches emerging from  $B_2$  and  $B'_2$  are connected and are the two ends of a same bridge, though a possible bridge breaking mechanism is not ruled out. We were not able to check this result numerically because the software used here could not follow bridges with such a complex structure.

## V. CHAOTIC SOLUTIONS

The stable periodic branches are eventually destabilized by a quasiperiodic branch, which itself is destabilized and leads to a chaotic regime. This is the sequence obtained numerically and displayed in Fig. 3(b). It is also clear from that picture that in general two or more attractors coexist. The lower of the chaotic branches in Fig. 3(b) exhibits a phenomenon that has been labeled low frequency fluctuations (LFFs) in semiconductor laser physics [37–42]. The time scales in semiconductor physics are extremely small. Therefore, all

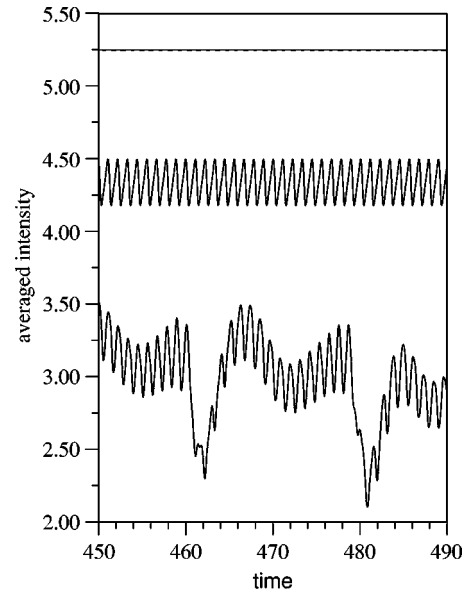


FIG. 6. Coexisting steady, periodic, and chaotic attractors for  $\eta=5.9$ ,  $\Omega=0$ ,  $\tau=1$ ,  $\alpha=3$ , and  $\tau_F=2$ .

the early experiments were made with oscilloscopes acting as low pass filters or time averaging devices. In a simplified model of that averaging effect, the recorded intensity  $I$  is related to the instantaneous intensity  $|E|^2$  by the equation

$$dI/dt = (|E|^2 - I)/\tau_F, \quad (27)$$

where  $\tau_F$  is the filter dimensionless time constant. The bandwidth of the filter (expressed in Hz) is equal to  $1/(\tau_F \tau_{ph} \tau)$ , where  $\tau_{ph}$  is the photon lifetime in the laser. It is only recently that streak cameras have been used to probe the dynamics of these lasers without significant averaging effect [40,43]. Typical values of  $\tau_F$  are of the order of unity,  $\tau \sim 10^3$  and  $\tau_{ph} \sim 10^{-12}$  s. In Fig. 5, we display the instantaneous (upper trace) and the averaged (lower trace) intensity for the point of the chaotic branch located at  $\eta=7.1$  in Fig. 3(b). It is a very neat example of LFF. The solution is composed of plateaus separated by gradual drop-offs and sharp recoveries. The duration between two consecutive drop-offs can reach a few hundred delay times. We have obtained LFF with plateaus lasting up to 388 delay times for Eq. (8) integrated with  $\eta=7.984$ ,  $p=-2.09$  (slightly below the threshold of the laser without feedback), and  $\alpha=2.5$ .

Increasing  $\eta$  along that branch of chaotic solutions, another chaotic attractor appears, and the solutions switch without any regularity between the two attractors. Increasing further  $\eta$ , only the new chaotic attractor is left. That attractor is of the classic type: it originates from a periodic attractor perturbed by a small amplitude chaos. However, on the next branch of chaotic solution, the chaos is quite different, being characterized by seemingly random spikes. Finally, we have verified numerically that replacing the cubic nonlinearity  $|E|^2 E$  by the nonlinearities  $|E|E$ ,  $|E|^3 E$ , and  $|E|^4 E$ , preserves the existence of LFF.

## VI. CONCLUSION

We have reduced asymptotically the Lang-Kobayashi equations (the full model) to the single cubic complex delay differential equation, Eq. (2). This equation has a bifurcation diagram of steady and periodic solutions, which displays all the complexity found in the full model. In particular, bridges of periodic solutions connecting two steady branches are still observed. The bifurcation diagram and the numerical simulations have been obtained with  $\alpha=3$ . This is a realistic value for semiconductor lasers today. Changing  $\alpha$  does not modify the topology of the bifurcation diagram, provided  $\alpha > 2/\pi$ . Below that critical value, pairs of branches emerging from the trivial solutions may be both supercritical, depending on  $\Omega$ . A characteristic of the bifurcation diagram displayed in Fig. 3(a) is that except for two small domains of the normalized feedback strength,  $1.81 < \eta < 1.86$  and  $3.70 < \eta < 3.86$ , there is always a stable steady state. Above the

first secondary bifurcation, coexistence of attractors is the rule. Numerically, bistability between steady state and chaotic states is easily found. In Fig. 6, multistability is illustrated for the section at  $\eta=5.9$  in the bifurcation diagram of Fig. 3(a) by showing three different coexisting attractors.

Beside the mechanism of bridge formation [20], a bridge destruction mechanism has also been identified for small values of  $\alpha$ . The asymptotic equation displays LFF. We have also verified numerically that equations of the type (1) with algebraic nonlinearities of the form  $|E|^n E$  with  $n=1,2,3$ , and 4 can also sustain LFF regimes. This suggests that LFF is a pervading property of DDEs rather than an exceptional feature of Eq. (1).

## ACKNOWLEDGMENT

This research has been supported by the Fonds National de la Recherche Scientifique and the Interuniversity Attraction Pole Program of the Belgian Government.

- 
- [1] K. Ikeda, *Opt. Commun.* **30**, 257 (1979).  
 [2] R. Lang and K. Kobayashi, *IEEE J. Quantum Electron.* **QE-16**, 347 (1980).  
 [3] I.R. Epstein, *Int. Rev. Phys. Chem.* **11**, 135 (1992).  
 [4] M. Roussel, *J. Phys. Chem.* **100**, 8323 (1996).  
 [5] E. Tziperman, L. Stone, M.A. Cane, and H. Jarosh, *Science* (Washington, DC, U.S.) **264**, 72 (1994).  
 [6] A.J. Clarke, X. Liu, and S. Van Gorder, *J. Clim.* **11**, 987 (1998).  
 [7] M.C. Mackey and L. Glass, *Science* (Washington, DC, U.S.) **197**, 287 (1977).  
 [8] A. Longtin, J.G. Milton, J.E. Bos, and M.C. Mackey, *Phys. Rev. A* **41**, 6992 (1990).  
 [9] M. Bando, K. Hasebe, K. Nakanishi, and A. Nakayama, *Phys. Rev. E* **58**, 5429 (1998).  
 [10] K. Nakanishi, *Phys. Rev. E* **62**, 3349 (2000).  
 [11] I. Luhta and I. Virtanen, *Chaos, Solitons Fractals* **7**, 2083 (1996).  
 [12] P.K. Asea and P.J. Zak, *J. Econ. Dyn. Control B* **23**, 1155 (1999).  
 [13] G.D. VanWiggeren and R. Roy, *Science* (Washington, DC, U.S.) **279**, 1198 (1998).  
 [14] J.P. Goedgebuer, L. Larger, and H. Porte, *Phys. Rev. Lett.* **80**, 2249 (1998).  
 [15] J.P. Goedgebuer, L. Larger, H. Porte, and F. Delorme, *Phys. Rev. E* **57**, 2795 (1998).  
 [16] G.D. VanWiggeren and R. Roy, *Int. J. Bifurcation Chaos* **9**, 2129 (1999).  
 [17] K. Cooke, P. van den Driessche, and X. Zou, *J. Math. Biol.* **39**, 332 (1999).  
 [18] K. Otsuka and J.L. Chern, *Opt. Lett.* **16**, 1759 (1991).  
 [19] F.T. Arecchi, G. Giacomelli, A. Lapucci, and R. Meucci, *Phys. Rev. A* **43**, 4997 (1991).  
 [20] D. Pieroux, T. Erneux, T. Luzyanina, and K. Engelborghs, *Phys. Rev. E* **63**, 036211 (2001).  
 [21] E.V. Grigorieva, H. Haken, and S.A. Kaschenko, *Opt. Commun.* **165**, 279 (1999).  
 [22] F.T. Arecchi, G. Giacomelli, A. Lapucci, and R. Meucci, *Phys. Rev. A* **45**, R4225 (1992).  
 [23] G. Giacomelli, R. Meucci, A. Politi, and F.T. Arecchi, *Phys. Rev. Lett.* **73**, 1099 (1994).  
 [24] G. Giacomelli and A. Politi, *Phys. Rev. Lett.* **76**, 2686 (1999).  
 [25] G. Giacomelli and A. Politi, *Physica D* **117**, 26 (1998).  
 [26] F. Kuwashima, I. Kitazima, and H. Iwasawa, *Jpn. J. Appl. Phys.* **37**, L325 (1998).  
 [27] F. Kuwashima, I. Kitazima, and H. Iwasawa, *Jpn. J. Appl. Phys.* **40**, 601 (2001).  
 [28] D. Pieroux *et al.*, *Phys. Rev. Lett.* **87**, 193901 (2001).  
 [29] K. Petermann, *IEEE J. Sel. Top. Quantum Electron.* **1**, 480 (1995).  
 [30] G. Huyet *et al.*, *Opt. Commun.* **180**, 339 (2000).  
 [31] T. Heil, I. Fischer, W. Elsäßer, and A. Gavrielides, *Phys. Rev. Lett.* **87**, 243901 (2001).  
 [32] D. Lenstra, M. Van Vaalen, and B. Jaskorzyńska, *Physica C* **125**, 255 (1984).  
 [33] G.H.M. van Tartwijk and D. Lenstra, *Quantum Semiclass. Opt.* **7**, 87 (1995).  
 [34] K. Engelborghs, K.U. Leuven Report No. TW-305 (unpublished).  
 [35] K. Engelborghs, T. Luzyanina, and D. Roose, *J. Comput. Appl. Math.* **125**, 265 (2000).  
 [36] E. Hairer, S.P. Nørsett, and G. Wanner, *Solving Ordinary Differential Equations*, 2nd ed. (Springer, Berlin, 1992), Vol.1. See also the site [www.cs.kuleuven.ac.be/~koen/delay/software.shtml](http://www.cs.kuleuven.ac.be/~koen/delay/software.shtml) for other softwares to solve DDEs.  
 [37] C. Risch and C. Voumard, *J. Appl. Phys.* **48**, 2083 (1977).  
 [38] I. Fischer *et al.*, *Phys. Rev. Lett.* **76**, 220 (1996).  
 [39] G. Huyet *et al.*, *Europhys. Lett.* **40**, 619 (1997).  
 [40] G. Vaschenko *et al.*, *Phys. Rev. Lett.* **81**, 5536 (1998).  
 [41] D.W. Sukow *et al.*, *Phys. Rev. A* **60**, 667 (1999).  
 [42] T. Heil *et al.*, *Opt. Lett.* **24**, 1275 (1999).  
 [43] G. Huyet *et al.*, *Opt. Commun.* **149**, 341 (1998).